Progress In Electromagnetics Research C, Vol. 74, 151–160, 2017

A Wideband Doherty Power Amplifier with Shunted Reactive Load for Efficiency Enhancement

Wa Kong[1], Jing Xia[1, 2, *], Da-Wei Ding[1], Li-Xia Yang[1], Chao Yu[3], and Yong-Zhao Zhan[1]

Abstract—A highly efficient Doherty power amplifier (DPA) using shunted reactive load is designed to achieve wideband operation. For enhanced back-off efficiency over the whole bandwidth, a modified load modulation network (LMN), which employs a shunted reactive load at the combining point, was firstly designed to enlarge the effective load impedance of the carrier amplifier at low and high frequencies. Then, the two-point matching approach was employed to design the carrier and peaking output matching networks, which can eliminate the use of offset lines and simplify the LMN. Measurement results show that the designed DPA can deliver an efficiency of 48%–61% at 6 dB back-off power over the frequency band of 2.2–2.9 GHz. For a 20 MHz LTE modulated signal, an average efficiency of higher than 55% can be achieved at an average output power of 37 dBm, while the adjacent channel leakage ratio is below −49 dBc after linearization.

1. INTRODUCTION

Future mobile communication systems adopt spectral efficient modulation schemes to achieve high transmission data rate, which results in time-varying signals with high peak-to-average power ratios (PAPRs). To efficiently amplify such time-varying signals, power amplifiers (PAs) need to provide high efficiency at large back-off powers. Moreover, for higher data throughput, an increasing number of frequency bands have been utilized in modern wireless standards. Thus, future PAs should be able to operate over a wide frequency range, satisfying the efficiency requirement when driven by wideband modulated signals.

To enhance the back-off efficiency, Doherty power amplifier (DPA) has been regarded as the most popular approach due to its significant efficiency enhancement and straightforward hardware implementation [1–8]. By actuating proper load modulation, these DPAs can maintain high efficiency at 6 dB or more back-off powers. However, in conventional DPA, the $\lambda_0/4$ impedance transformer after the carrier amplifier limits the bandwidth [9]. Because of the dispersion effect of the transmission line, the effective carrier load impedance in the low power region will decrease dramatically when the frequency deviates from the center frequency of f_0. This results in the degradation of back-off efficiency and limits the bandwidth of the DPA. Although several designs have been proposed to extend the bandwidth [10–22], many of them are still complicated for realization. Recently, a novel output combiner employing a resonance LC tank was reported in the frequency band of 0.7–0.95 GHz [15]. However, it is hard to use this topology in higher operation frequency band.

In this article, a 2.2–2.9 GHz high efficiency DPA using a shunt reactive load (SRL) in the combining network is reported. In the proposed load modulation network (LMN), the shunt reactive load, which is designed using open-circuit stepped impedance transmission lines, is connected to the combining point

Received 17 March 2017, Accepted 15 May 2017, Scheduled 30 May 2017

* Corresponding author: Jing Xia (ujsasan@gmail.com).

[1] School of Computer Science and Communication Engineering, Jiangsu University, Zhenjiang 212013, China. [2] Jingjiang College, Jiangsu University, Zhenjiang 212013, China. [3] State Key Laboratory of Millimeter Waves, Southeast University, Nanjing 210096, China.

(CP) to enlarge the effective back-off load impedances and the efficiency of the carrier amplifier at low and high frequencies. In addition, the frequency dispersion of the effective load impedance can be alleviated by eliminating conventional offset lines when using the two-point matching output matching network (OMN). Theoretical analysis of the proposed approach is given. The efficiency enhancement of the proposed method was validated compared with conventional design. Experimental results of the output power and efficiency of the designed DPA, as well as the linearization results, are also presented.

2. ANALYSIS OF PROPOSED DPA FOR BANDWIDTH ENHANCEMENT

The simplified schematics of the DPAs with conventional and proposed LMN are shown in Fig. 1. A modified LMN, including two $\lambda_0/4$ impedance transformers (ITs) and a shunted reactive load, is employed in the proposed DPA for efficiency enhancement and bandwidth extension.

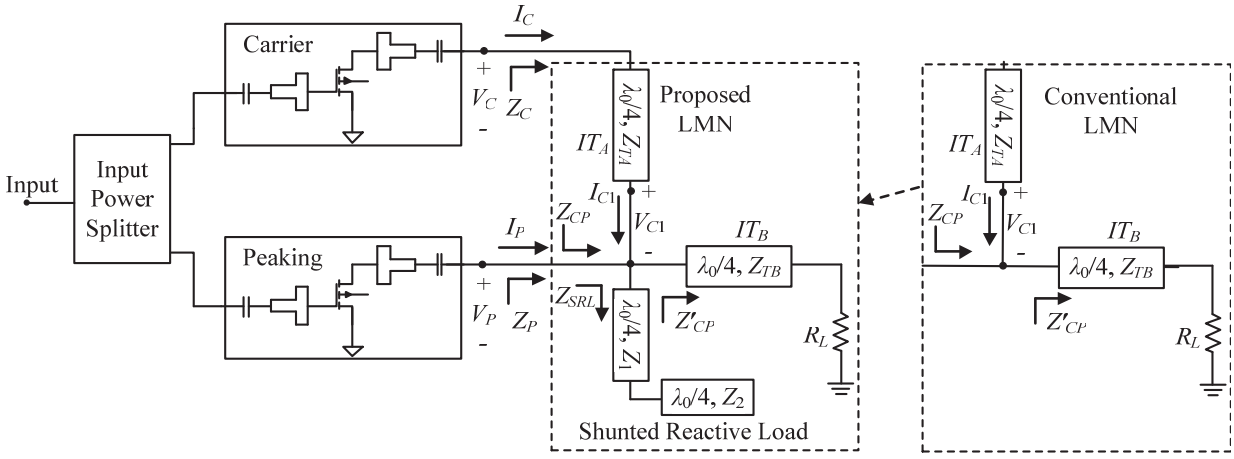

Figure 1. The simplified schematics of the DPAs with conventional and proposed LMN.

When input power is low (low power region), the peaking amplifier in the off-state is open-circuited seen from the combining point. So, the output impedance of IT_A turns to be Z_{CP}. The effective load impedances of the carrier and peaking amplifiers in the low power region at a given frequency can be given by [9]

$$Z_{C\_low} = Z_{TA}\frac{Z_{CP} + jZ_{TA}\tan\beta l}{Z_{TA} + jZ_{CP}\tan\beta l} \tag{1}$$

$$Z_{P\_low} = \infty \tag{2}$$

where βl is the phase delay of the transmission line at a given frequency f, and it is given by

$$\beta l = \frac{f}{f_0}\cdot\frac{\pi}{2} \tag{3}$$

When input power increases (the Doherty region), considering the $ABCD$ matrix of IT_A, the fundamental voltage and current of the carrier amplifier can be expressed as

$$\begin{bmatrix} V_C \\ I_C \end{bmatrix} = \begin{bmatrix} \cos\beta l & jZ_{TA}\sin\beta l \\ j\dfrac{\sin\beta l}{Z_{TA}} & \cos\beta l \end{bmatrix} \begin{bmatrix} V_{C1} \\ I_{C1} \end{bmatrix} \tag{4}$$

From Fig. 1, the fundamental voltage of the peaking amplifier is given by

$$V_P = V_{C1} = I_{C1}Z_{CP} \tag{5}$$

According to Eqs. (4) and (5), the following relationships arise:

$$I_{C1} = \frac{V_P}{Z_{CP}} = \frac{V_C}{Z_{CP}\cos\beta l + jZ_{TA}\sin\beta l} \tag{6}$$

$$V_P = \frac{V_C Z_{CP}}{Z_{CP}\cos\beta l + jZ_{TA}\sin\beta l} \tag{7}$$

Using Eq. (6), the following expression can be obtained according to the active load modulation.

$$Z_{C1} = Z_{CP}\left(1 + \frac{I_P}{I_{C1}}\right) = Z_{CP}\frac{V_C + jI_P Z_{TA}\sin\beta l}{V_C - Z_{CP}I_P\cos\beta l} \tag{8}$$

According to the impedance transformation of IT_A, the output voltage of the carrier amplifier becomes

$$V_C = I_C Z_C = I_C \frac{Z_{C1}\cos\beta l + jZ_{TA}\sin\beta l}{Z_{C1}j\dfrac{\sin\beta l}{Z_{TA}} + \cos\beta l} \tag{9}$$

Substituting Eqs. (8) into (9) results in the following expression

$$V_C = \frac{Z_{TA}Z_{CP}(I_C\cos\beta l + I_P) + jI_C Z_{TA}^2\sin\beta l}{Z_{TA}\cos\beta l + jZ_{CP}\sin\beta l} \tag{10}$$

When the input power is high, the output powers of the carrier and peaking amplifiers reach saturation. From Eq. (10), the modulated load impedance seen by the carrier amplifier at saturation power can be written as

$$Z_{C\_sat} = \frac{V_C}{I_C} = \frac{Z_{TA}Z_{CP}\left(\cos\beta l + \delta e^{j\phi}\right) + jZ_{TA}^2\sin\beta l}{Z_{TA}\cos\beta l + jZ_{CP}\sin\beta l} \tag{11}$$

where δ is the current ratio and can be expressed as $\delta = |I_{P\_sat}|/|I_{C\_sat}|$, and ϕ is the phase delay between the output current of the peaking and carrier amplifiers.

By means of the equations from Eqs. (7) to (9), the modulated load impedance seen by the peaking amplifier at saturation power is given by

$$Z_{P\_sat} = \frac{V_P}{I_P} = \frac{Z_{TA}Z_{CP}\left(e^{-j\phi} + \delta\cos\beta l\right)}{\delta(Z_{TA}\cos\beta l + jZ_{CP}\sin\beta l)} \tag{12}$$

According to Fig. 1, for conventional DPA, the load impedance seen at the combining point Z_{CP} is given by

$$Z_{CP} = Z'_{CP} = Z_{TB}\frac{R_L + jZ_{TB}\tan\beta l}{Z_{TB} + jR_L\tan\beta l} \tag{13}$$

In a general case, R_L is $50\,\Omega$. Assuming $Z_{TA} = 50\,\Omega$, $Z_{TB} = 35.35\,\Omega$, $\delta = 1$ and $\phi = -\beta l$, the load impedances of the two amplifiers in conventional DPA at both low power region and saturation can be calculated according to Eqs. (1), (2), (11), (12) and (13), as shown in Figs. 2 and 3. It is shown that, for conventional DPA, the resistance of the carrier load impedance in low power region and the load impedances of the two amplifiers at saturation, decrease dramatically as the frequency deviates from f_0, leading to bandwidth limitation and improper load modulation.

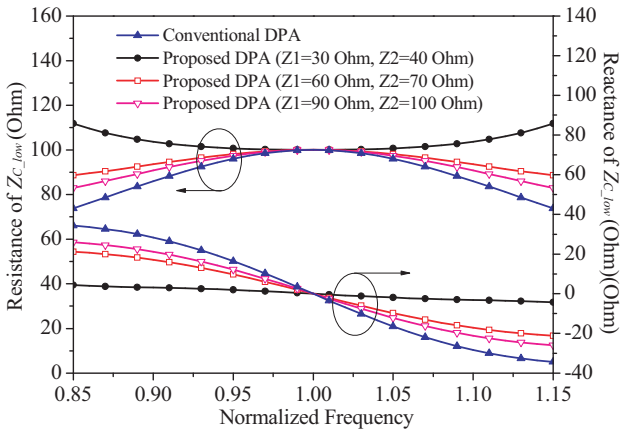

Figure 2. Carrier load impedance of conventional and proposed DPA in low power region.

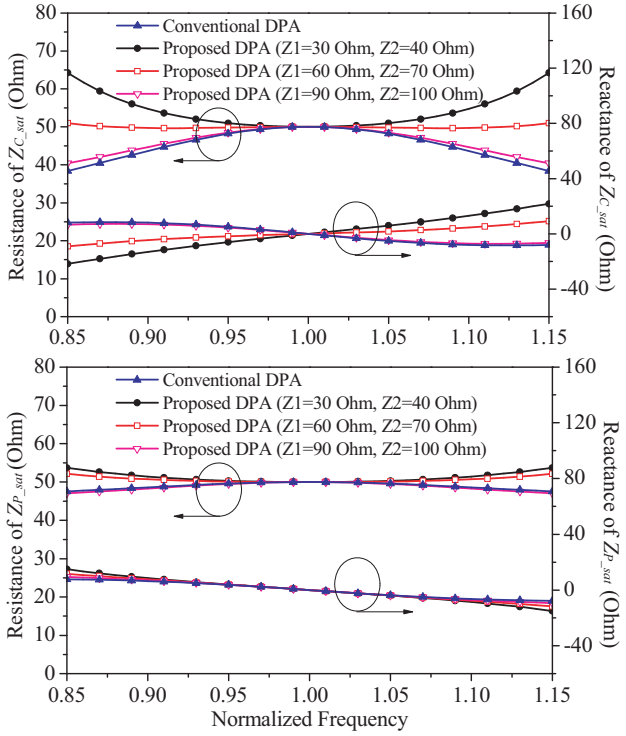

Figure 3. Carrier and peaking load impedances of conventional and proposed DPA at saturation.

To solve this problem, several kinds of reactive loads can be connected at the combining point. In this paper, the shunted reactive load is designed with an open-circuited structure consisting of two $\lambda_0/4$ transmission lines. Then, for the proposed DPA, the load impedance Z_{CP} can be expressed as

$$Z_{CP} = Z'_{CP}//Z_{SRL} \tag{14}$$

$$Z_{SRL} = jZ_1\frac{Z_1\tan^2\beta l - Z_2}{(Z_1+Z_2)\tan\beta l} \tag{15}$$

According to Eqs. (1), (2) and (11)–(15), the carrier and peaking load impedances in the proposed DPA depend on the characteristic impedances of the two transmission lines (Z_1 and Z_2). For comparison, three kinds of the proposed LMNs with different Z_1 and Z_2 are simulated. The load impedances are also depicted in Figs. 2 and 3.

It can be observed that, with the help of appropriate shunted reactive load Z_{SRL} ($Z_1 = 60\,\Omega$, $Z_2 = 70\,\Omega$ and the length of the two transmission lines are both $\lambda_0/4$), the resistance of the carrier load impedance in the low power region can be effectively enlarged to be close to $100\,\Omega$ at low and high frequencies. Meanwhile, the load modulation at saturation can also be improved with the resistances closer to $50\,\Omega$ over the whole frequency band. Thus, the efficiency and bandwidth of the DPA can be effectively enhanced by employing the proposed topology.

3. CIRCUIT DESIGN AND SIMULATIONS

For verification of the proposed approach, a wideband high efficiency DPA with shunted reactive load was designed and simulated using the large signal model of Cree CGH40010F GaN transistor over the frequency band of 2.2–2.9 GHz. The carrier amplifier was biased at a deep class AB mode with $I_{DS} = 0.05$ A, while the peaking amplifier was in class C operation with $V_{GS} = -6$ V. To improve the load modulation, the drain voltage of the carrier and peaking amplifiers were set to 24 and 28 V so that the peaking amplifier can achieve similar output power with the carrier amplifier at saturation.

To achieve desired Doherty behavior, the simplified model of the carrier and peaking OMNs in the proposed DPA is shown in Fig. 4. In this schematic, Z_{dC_low} and Z_{dC_sat} represent the optimum drain

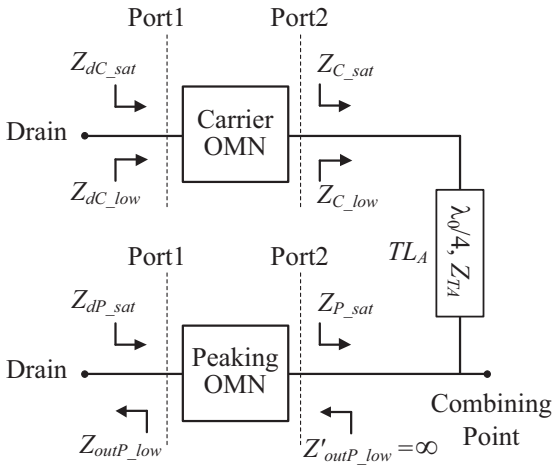

Figure 4. Simplified model of carrier and peaking OMNs.

load seen by the carrier device at the low power region and saturation, while Z_{outP_low} and Z_{dP_sat} denote the output impedance and optimum drain load of the peaking device respectively. In the low power region, impedance Z_{C_low} is transformed to Z_{dC_low} in the carrier OMN, while Z_{outC_low} is transformed to open circuit in the peaking OMN. On the other hand, at saturation, the impedances Z_{C_sat} and Z_{P_sat} are transformed to Z_{dC_sat} and Z_{dP_sat}, respectively.

By using load pull simulations, the desired impedances for the carrier and peaking OMNs are given in Tables 1 and 2. To achieve the design targets mentioned above, the two-point matching approach proposed in [21] can be employed. Taking the carrier OMN design for example, by using S_{11} and the phase of S_{21} (θ_{21}) of the carrier OMN, the relationships between the load impedances, i.e., Z_{C_sat}, Z_{dC_sat}, Z_{C_low} and Z_{dC_low}, can be expressed as

$$\frac{Z_0 Z_{C\_sat} a + Z_0^2 b + Z_0 (Z_{C\_sat} - Z_0) c}{Z_{dC\_sat} Z_{C\_sat} d + Z_{dC\_sat} Z_0 e + Z_{dC\_sat} (Z_0 - Z_{C\_sat}) c} = 1 \tag{16}$$

$$\frac{Z_0 Z_{C\_low} a + Z_0^2 b + Z_0 (Z_{C\_low} - Z_0) c}{Z_{dC\_low} Z_{C\_low} d + Z_{dC\_low} Z_0 e + Z_{dC\_low} (Z_0 - Z_{C\_low}) c} = 1 \tag{17}$$

where Z_0 is the reference impedance, and

$$a = (1 + S_{11})(1 + S_{11}^* e^{j2\theta_{21}}) \quad b = (1 + S_{11})(1 - S_{11}^* e^{j2\theta_{21}}) \quad c = (1 - |S_{11}|^2) e^{j2\theta_{21}}$$

Table 1. Design parameters of the carrier OMN.

Frequency (GHz)	Z_{dC_low}	Z_{C_low}	Z_{dC_sat}	Z_{C_sat}	θ_{21_C}
2.2	$13 + j13\,\Omega$	$100\,\Omega$	$19 + j4\,\Omega$	$50\,\Omega$	$-128°$
2.55	$22 + j19\,\Omega$	$100\,\Omega$	$18.5 + j5\,\Omega$	$50\,\Omega$	$-154°$
2.9	$35 + j11\,\Omega$	$100\,\Omega$	$18 + j6\,\Omega$	$50\,\Omega$	$-180°$

Table 2. Design parameters of the peaking OMN.

Frequency (GHz)	Z_{outP_low}	Z'_{outP_low}	Z_{dP_sat}	Z_{P_sat}	θ_{21_P}
2.2	$0.5 - j43\,\Omega$	Quasi-open	$19 + j4\,\Omega$	$50\,\Omega$	$-129°$
2.55	$0.5 - j35\,\Omega$	Open	$18.5 + j5\,\Omega$	$50\,\Omega$	$-153°$
2.9	$0.5 - j28\,\Omega$	Quasi-open	$18 + j6\,\Omega$	$50\,\Omega$	$-178°$

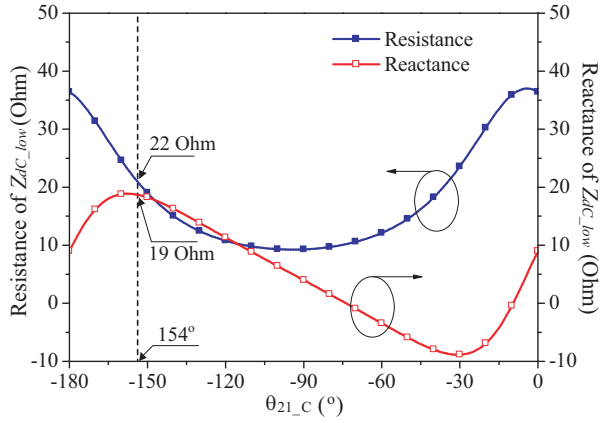

Figure 5. Graphical illustration of the matching technique for the carrier OMN at the frequency of 2.55 GHz.

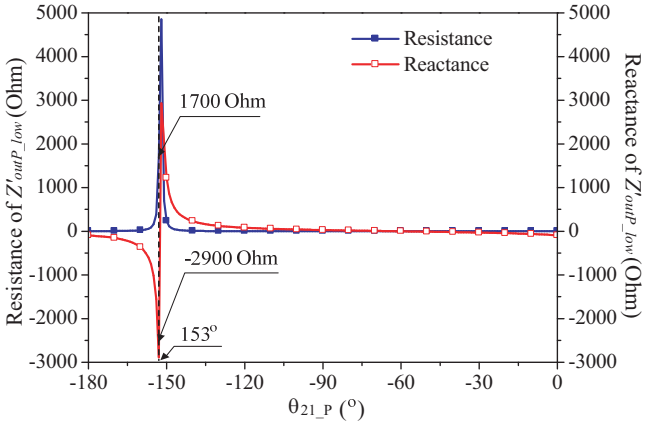

Figure 6. Graphical illustration of the matching technique for the peaking OMN at the frequency of 2.55 GHz.

$$d = (1 - S_{11})(1 + S_{11}^{*} e^{j2\theta_{21}}) \quad e = (1 - S_{11})(1 - S_{11}^{*} e^{j2\theta_{21}})$$

For the carrier OMN design at the frequency of 2.55 GHz, by using three impedances, i.e., Z_{C_low}, Z_{dC_sat} and Z_{C_low}, the impedance Z_{dC_low} can be expressed as a function of θ_{21_C} according to (16) and (17), as depicted in Fig. 5. The anticipated θ_{21_C} can be determined to be $-154°$ according to the result where Z_{dC_low} is close to the desired value of $22 + j19\,\Omega$. The calculated values of θ_{21_C} at 2.2, 2.55 and 2.9 GHz are also shown in Table 1. Similar approach can also be used to estimate θ_{21_P}, as also depicted in Fig. 6 and Table 2.

According to those design parameters, the carrier and peaking OMNs can be synthesized by network theory and tuned by using computer optimization. The final topology of the designed OMNs and modified LMN is shown in Fig. 7. Because the calculated S_{21} phase of the carrier and peaking OMNs are similar, same matching topology is used in the OMN designs. It should be noted that, with the two-point matching approach, ideal load modulation can be achieved without the use of the offset lines, which are usually used in conventional DPA. Then, the output network of the DPA can be simplified, leading to performance improvement. For the proposed DPA design, the input matching networks (IMNs) were designed using the stepped-impedance matching network topology to cover the required bandwidth. A 3 dB 90° hybrid coupler was used as the input power splitter.

In Fig. 8, the simulated drain efficiencies (DEs) as well as the saturated output power are depicted. The DE is between 48%–66% at 6 dB back-off power, and is between 57%–75% at saturation. Regarding the saturated output power, it is higher than 43.5 dBm over the whole frequency band. For comparative purpose, the 6 dB back-off efficiency of a conventional DPA without the shunted reactive load was also simulated and depicted. It can be observed that about 5% efficiency enhancement can be achieved using the proposed approach at low operation frequency.

4. REALIZATION AND EXPERIMENTAL RESULTS

For experimental validation of the proposed design, the DPA with shunted reactive load was built on a Taconic RF35 substrate with $\varepsilon_r = 3.55$ and thickness of 30 mil, as shown in Fig. 9. To improve the load modulation, different drain voltages were employed to make the peaking amplifier to achieve similar power with the carrier amplifier.

Figure 10 shows the DE and gain of the DPA at peak output power and 6 dB back-off power versus frequency under continuous wave (CW) measurements. The proposed DPA delivers 48%–61% DE at 6 dB back-off power from 2.2 to 2.9 GHz. The measured DE and gain characteristics as a function of output power at the frequencies of 2.2, 2.4, 2.7 and 2.9 GHz were depicted in Fig. 11. It can be seen that the DE, gain and output power maintain appropriate consistency at different frequencies across large

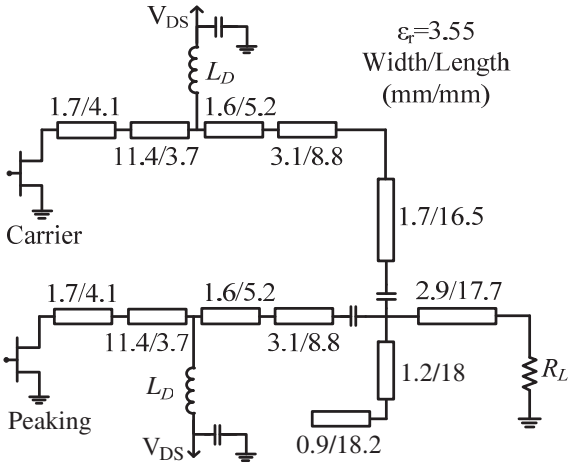

Figure 7. Final topology of the designed OMNs and modified LMN.

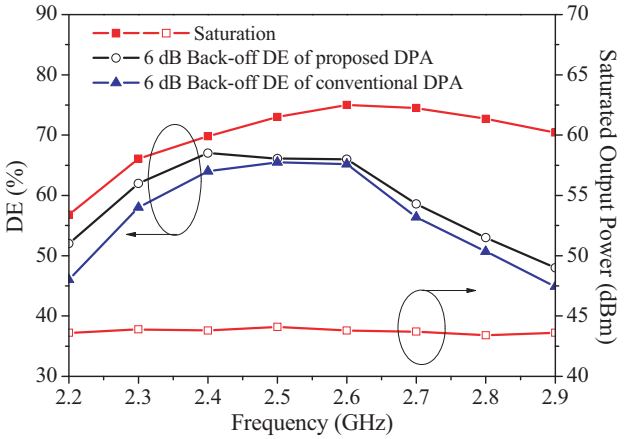

Figure 8. Simulated efficiencies and saturated output power of proposed DPA and conventional DPA over the frequency band of 2.2–2.9 GHz.

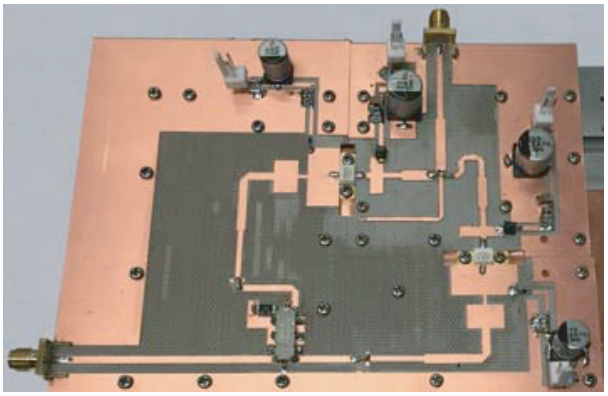

Figure 9. Photograph of the designed DPA.

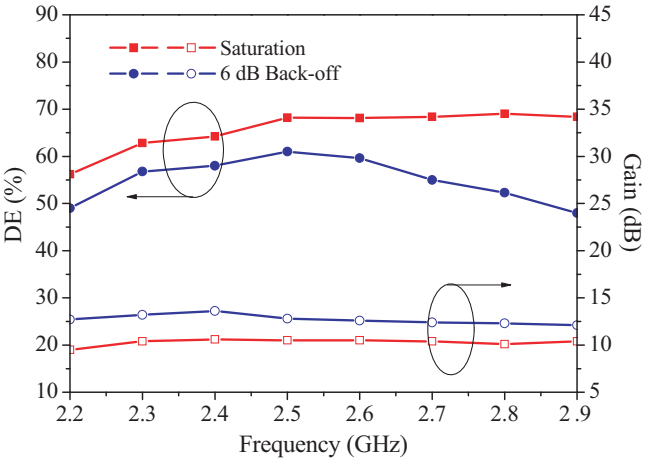

Figure 10. Measured DE and gain of the DPA versus frequency at saturation, and 6 dB back-off powers.

back-off range. The saturation output power was found to be more than 43.5 dBm with associated DE of higher than 56%. High efficiency in large back-off power range and Doherty type efficiency profiles can also be observed.

To validate the linearity performance, the DPA was driven by a 20 MHz LTE signal with PAPR about 7 dB at the carrier frequency of 2.55 GHz, and then was linearized by using the digital predistortion (DPD) technique [21]. Fig. 12 shows the measured spectra before and after DPD for 20 MHz modulated signal at an average output power of 37 dBm with an efficiency of 55%. The adjacent channel leakage ratio (ACLR) is −33 and −49 dBc before and after DPD, respectively. The designed DPA can operate efficiently at back-off powers with high linearity. Table 3 shows the performance comparison with the published wideband DPAs. Especially for higher operational frequency, the proposed DPA exhibits a higher efficiency at back-off power and high output power for wideband operations, compared with most solutions using packaged devices.

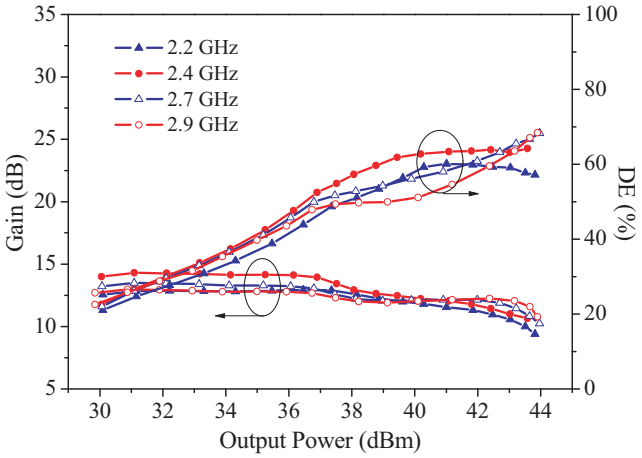

Figure 11. Measured DE and gain versus output power at different frequencies.

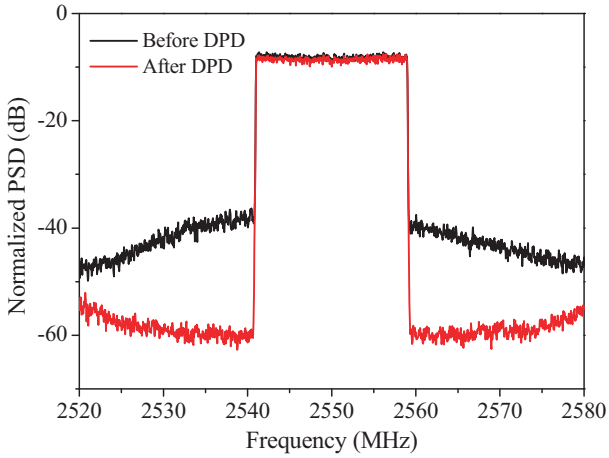

Figure 12. Measured spectra of the DPA at an output power of 37 dBm before and after DPD.

Table 3. Performance comparison with previous works.

Ref.	Year	Device	Frequency (GHz)	Pout (dBm)	DE at 6 dB back-off power (%)	DE at saturated power (%)
[11]	2012	Packaged	3–3.6	43	38–56	55–65
[12]	2012	Packaged	1.96–2.46	40	40–44	46–60
[14]	2013	Bare-die	1.67–2.41	41	43–59	53–72
[15]	2014	Packaged	0.7–0.95	43	48–57	53–67
[16]	2014	Bare-die	1.05–2.55	42	35–58	45–83
[18]	2015	Packaged	2.0–2.7	40.5	35–65	58–70
[19]	2015	Packaged	1.6–2.4	42.7	55–63	72–77
[20]	2015	Packaged	1.7–2.6	44.6	47–57	57–66
[22]	2016	Packaged	1.72–2.27	42.5	48–55	58–72
This work	2017	Packaged	2.2–2.9	43.5	48–61	56–70

5. CONCLUSIONS

In this paper, the design of a high efficiency GaN DPA with operation bandwidth of 2.2–2.9 GHz is reported. A modified LMN with shunted reactive load is employed to enhance back-off efficiency. Experiment results show that the proposed DPA has good efficiency performance over wide frequency band.

ACKNOWLEDGMENT

This work was supported by the Natural Science Foundation of Jiangsu Province of China under Grant No. BK20150528 and the Natural Science Foundation of the Jiangsu Higher Education Institutions of China under Grant Nos. 15KJB510007 and 16KJB510006. This work was also supported by the Research Foundation for Advanced Talents of Jiangsu University under Grant No. 15JDG080.

REFERENCES

1. Chen, S. and Q. Xue, "Optimized load modulation network for Doherty power amplifier performance enhancement," *IEEE Transactions on Microwave Theory and Techniques*, Vol. 60, No. 11, 3474–3481, Nov. 2012.
2. Fan, C. Z., X. W. Zhu, J. Xia, and L. Zhang, "Efficiency enhanced class-F Doherty power amplifier at 3.5 GHz for LTE-advanced application," *Asia-Pacific Microwave Conference (APMC)*, 707–709, Seoul, 2013.
3. Xia, J., X. Zhu, L. Zhang, J. Zhai, and Y. Sun, "High-efficiency GaN Doherty power amplifier for 100 MHz LTE-advanced application based on modified load modulation network," *IEEE Transactions on Microwave Theory and Techniques,* Vol. 61, No. 8, 2911–2921, Aug. 2013.
4. Nghiem, X. A. and R. Negra, "Design of a concurrent quad-band GaN-HEMT Doherty power amplifier for wireless applications," *IEEE MTT-S International Microwave Symposium Digest*, 1–4, Seattle, WA, USA, Jun. 2013.
5. Özen, M. and C. Fager, "Symmetrical Doherty amplifier with high efficiency over large output power dynamic range," *IEEE MTT-S International Microwave Symposium Digest*, 1–3, Tampa, FL, USA, Jun. 2014.
6. Camarchia, V., S. Donati Guerrieri, G. Ghione, et al., "A K band GaAs MMIC Doherty power amplifier for point to point microwave backhaul applications," *International Workshop on Integrated Nonlinear Microwave and Millimetre-Wave Circuits (INMMiC'14)*, 1–3, Leuven, Belgium, Apr. 2014.
7. Xia, J. and X. Zhu, "Doherty power amplifier with enhanced in-band load modulation for 100 MHz LTE-advanced application," *Microwave and Optical Technology Letters*, Vol. 57, No. 2, 391–395, Feb. 2015.
8. Park, Y., J. Lee, S. Jee, S. Kim, and B. Kim, "Optimized Doherty power amplifier with a new offset line," *IEEE MTT-S International Microwave Symposium Digest*, 1–4, Phoenix, AZ, USA, Jun. 2015.
9. Bathich, K., A. Z. Markos, and G. Boeck, "Frequency response analysis and bandwidth extension of the Doherty amplifier," *IEEE Transactions on Microwave Theory and Techniques*, Vol. 59, No. 4, 934–944, Apr. 2011.
10. Kang, D., D. Kim, Y. Cho, B. Park, J. Kim, and B. Kim, "Design of bandwidth-enhanced Doherty power amplifiers for handset applications," *IEEE Transactions on Microwave Theory and Techniques*, Vol. 59, No. 12, 3474–3483, Dec. 2011.
11. Rubio, J. M., J. Fang, V. Camarchia, R. Quaglia, M. Pirola, and G. Ghione, "3–3.6 GHz wideband GaN Doherty power amplifier exploiting output compensation stages," *IEEE Transactions on Microwave Theory and Techniques*, Vol. 60, No. 8, 2543–2548, Aug. 2012.
12. Akbarpour, M., M. Helaoui, and F. M. Ghannouchi, "A transformerless load-modulated (TLLM) architecture for efficient wideband power amplifiers," *IEEE Transactions on Microwave Theory and Techniques*, Vol. 60, No. 9, 2863–2874, Sep. 2012.
13. Seo, M., H. Lee, J. Gu, and Y. Yang, "Doherty power amplifier using a compact load network for bandwidth extension," *Asia-Pacific Microwave Conference (APMC)*, 742–744, Seoul, 2013.
14. Piazzon, L., P. Colantonio, R. Giofrè, and F. Giannini, "A wideband Doherty architecture with 36% of fractional bandwidth," *IEEE Microwave Wireless Components Letters*, Vol. 23, No. 11, 626–628, Nov. 2013.
15. Abadi, M. N. A., H. Golestaneh, H. Sarbishaei, and S. Boumaiza, "An extended bandwidth Doherty power amplifier using a novel output combining," *IEEE MTT-S International Microwave Symposium Digest*, 1–3, Tampa, FL, USA, Jun. 2014.
16. Giofrè, R., L. Piazzon, P. Colantonio, and F. Giannini, "An ultra-broadband GaN Doherty amplifier with 83% of fractional bandwidth," *IEEE Microwave Wireless Components Letters*, Vol. 24, No. 11, 775–777, Nov. 2014.
17. Watanabe, S., Y. Takayama, R. Ishikawa, and K. Honjo, "A miniature broadband Doherty power amplifier with a series-connected load," *IEEE Transactions on Microwave Theory and Techniques*,

Vol. 63, No. 2, 572–579, Feb. 2015.

18. Nghiem, X. A., J. Guan, and R. Negra, "Broadband sequential power amplifier with Doherty-type active load modulation," *IEEE Transactions on Microwave Theory and Techniques*, Vol. 63, No. 9, 2821–2832, Sep. 2015.
19. Fang, X. H. and K. K. M. Cheng, "Improving power utilization factor of broadband Doherty amplifier by using bandpass auxiliary transformer," *IEEE Transactions on Microwave Theory and Techniques*, Vol. 63, No. 9, 2811–2820, Sep. 2015.
20. Pang, J., S. He, C. Huang, Z. Dai, J. Peng, and F. You, "A post-matching Doherty power amplifier employing low-order impedance inverters for broadband applications," *IEEE Transactions on Microwave Theory and Techniques*, Vol. 63, No. 12, 4061–4071, Dec. 2015.
21. Xia, J., M. Yang, Y. Guo, and A. Zhu, "A broadband high-efficiency Doherty power amplifier with integrated compensating reactance," *IEEE Transactions on Microwave Theory and Techniques*, Vol. 64, No. 7, 2014–2024, Jul. 2016.
22. Abadi, M. N. A., H. Golestaneh, H. Sarbishaei, and S. Boumaiza, "Doherty power amplifier with extended bandwidth and improved linearizability under carrier-aggregated signal stimuli," *IEEE Microwave Wireless Components Letters*, Vol. 26, No. 5, 358–360, May 2016.